INSTITUTE OF PHYSICS PUBLISHING NANOTECHNOLOGY
Nanotechnology **18** (2007) 055702 (7pp) doi:10.1088/0957-4484/18/5/055702

A parametric study of $TiO_2/CuInS_2$ nanocomposite solar cells: how cell thickness, buffer layer thickness, and TiO_2 particle size affect performance

Ryan O'Hayre[1,3], Marian Nanu[2], Joop Schoonman[2] and Albert Goossens[2]

[1] Department of Metallurgical and Materials Engineering, Colorado School of Mines, 1500 Illinois St. Golden, CO 80401, USA
[2] Delft Institute for Sustainable Energy, Delft University of Technology, 2628 BL Delft, The Netherlands

E-mail: rohayre@mines.edu

Received 10 July 2006, in final form 25 October 2006
Published 9 January 2007
Online at stacks.iop.org/Nano/18/055702

Abstract
3D $CuInS_2/TiO_2$ nanocomposite solar cell performance is strongly influenced by several structural factors, including cell thickness, buffer layer thickness, and the morphology of the TiO_2 nanoparticulate matrix. To delineate the effect of these structural factors on photovoltaic performance, a series of parametric studies are performed where a single structural parameter is varied (TiO_2 nanoparticulate matrix thickness, In_2S_3 buffer layer thickness, or TiO_2 particle size) while all other fabrication conditions are held constant. The best overall performance (3.0% efficiency at AM 1.5) is achieved from a device with TiO_2 matrix thickness $\approx$200 nm, In_2S_3 buffer layer thickness $\approx$60 nm, and TiO_2 nanoparticulate size $=$ 300 nm. Notably, the film thickness in the best-performing cell (200 nm) is less than the TiO_2 particle size (300 nm), corresponding to a discontinuous nanoparticulate film. Thicker TiO_2 nanoparticulate films or smaller TiO_2 particles sizes lead to decreased performance due to increased charge transport resistance. However, the performance from a planar cell (where the TiO_2 nanoparticulate layer is not used) is inferior to the performance from the better-optimized 3D cells, indicating that some degree of nanostructuring improves performance. Device performance is also observed to depend strongly on In_2S_3 buffer layer thickness, with optimal performance achieved for a buffer layer thickness of approximately 60 nm. The optimal buffer layer thickness is governed by two opposing factors: increasing the buffer layer thickness improves the interfacial characteristics (as measured by decreasing leakage conductance, G) but also screens the incoming light and causes an increase in the charge transport resistance (as measured by the cell series resistance, R_s).

(Some figures in this article are in colour only in the electronic version)

1. Introduction

Photovoltaic designs based on nanostructured materials offer an intriguing route towards inexpensive, reliable, solar-based renewable power. Research by Grätzel *et al* [1], Heeger *et al* [2], and others [3–5] has produced a variety of successful solar cell designs using nanometre scale blends or interpenetrating systems. While most of the nanostructured solar cell designs use dye/electrolyte couples and/or organic

[3] Author to whom any correspondence should be addressed.

materials, inorganic designs are desirable to obviate leakage, sealing, and degradation concerns. Among the inorganic nanostructured solar cell concepts, the extremely-thin absorber (ETA) cell [6–9] has been particularly successful. The 3D nanostructured TiO_2/CIS solar cell, based on a nanoscale interpenetrating structure between n-type TiO_2 and p-type $CuInS_2$ (CIS), is a relatively recent inorganic-based design in this field [10]. The operating principle of the 3D nanostructured TiO_2/CIS solar cell is analogous to a traditional thin-film CIS solar cell. However, compared to a planar device, the nanostructured interface between the p-type CIS layer and the n-type TiO_2 matrix shortens the average minority carrier diffusion length, thereby improving the collection efficiency and providing the device with a higher tolerance to defects and impurities. Like most chalcopyrite solar cells, a buffer layer is typically required between the n-type and p-type regions to control the interfacial properties. In the present 3D nanocomposite solar cells, a thin In_2S_3 buffer layer is used between the TiO_2 and CIS layers. The buffer layer is particularly important for 3D nanocomposite solar cells because the large interfacial junction area increases the probability of recombination [11].

TiO_2/CIS nanocomposite solar cells have achieved greater than 5% energy conversion efficiency under simulated AM 1.5 irradiation [12]. However, deployment of a 3D hetero-interface increases the structural complexity of the TiO_2/CIS solar cell device. Performance is particularly sensitive to the size of the TiO_2 particles used [13], the thickness of the nanostructured TiO_2 layer [14], and the effectiveness of the buffer layer passivation [11, 15–17]. In order to examine the impact of these structural factors on photovoltaic performance, a series of parametric studies have been performed. In these studies, a single structural parameter is varied while all other solar cell fabrication conditions are held constant. Three structural parameters are investigated:

(1) TiO_2 nanoparticulate matrix thickness,
(2) TiO_2 particle size,
(3) In_2S_3 buffer layer thickness.

Figure 1 schematically identifies each of the three investigated structural parameters. Eleven separate samples are investigated. Table 1 provides the structural details for all 11 samples.

2. Experimental details

The fabrication of TiO_2/CIS nanocomposite solar cells is discussed extensively in [12]. The process is briefly summarized here. First, a dense film of anatase TiO_2 (approx. 150 nm) is deposited onto transparent conducting oxide (TCO, LOF Tec 10) glass substrates using chemical spray pyrolysis. This dense layer of spray-deposited TiO_2 is provisioned to all samples to ensure against shorting. Next, a nanocrystalline anatase-TiO_2 coating is applied using the doctor-blade technique. For the thickness study, samples with nanocrystalline TiO_2 layer thicknesses of 0, 150, 300 and 1200 nm respectively are prepared by systematically varying the viscosity of the precursor paste (via dilution with ethanol). The 'planar' sample with 0 nm of nanocrystalline TiO_2 contained only the sprayed base layer of dense TiO_2.

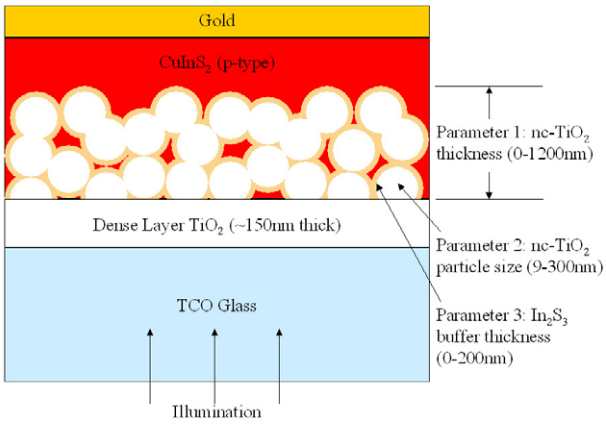

Figure 1. A schematic drawing of the TiO_2/CIS 3D nanostructured solar cell. The three structural factors chosen for parametric study are identified on the drawing. Parameter 1: the thickness of the nanocrystalline TiO_2 layer. Parameter 2: the size of the TiO_2 nanoparticles used in the nanocrystalline layer. Parameter 3: the thickness of the In_2S_3 buffer layer applied between the nanocrystalline TiO_2 particles and the CIS absorber layer. All other parameters, such as the processing temperatures and chemistries, the thickness of the dense TiO_2 layer, the thickness of the CIS absorber layer, and the thickness and size of the gold top electrode are held constant.

This sample thus represents the limiting condition of device performance in the absence of nanostructuring. For the particle size study, samples containing 9, 50, and 300 nm anatase-TiO_2 crystallites, respectively, are prepared by using different precursor pastes (9, 50, and 300 nm precursor pastes, all commercially available from Solaronix, Inc.). After doctor blading, all samples are annealed at 450 °C for 6 h in air. The samples are then coated with a spray-deposited n-type In_2S_3 buffer layer. The standard In_2S_3 deposition sequence (12 spray cycles) provides a 50 nm thick buffer layer. However, for the In_2S_3 buffer layer thickness study, samples are coated with 0, 20, 60, or 200 nm of In_2S_3 by varying the number of spray-deposition cycles (0, 5, 15, or 45 spray cycles respectively). Following buffer layer deposition, all samples are spray coated with p-type $CuInS_2$ [18]. In all samples, the CIS layer thickness is held approximately constant (by using a standardized 20-cycle spray deposition procedure) at approximately 500 nm thick. To define test cells (0.0314 cm^2 in area), gold contacts are evaporated on top of the CIS layer. In all electrical measurements, the gold/CIS electrode served as the working electrode, while the TCO/TiO_2 electrode served as the counter/reference electrode. Thus in forward bias, the CIS layer was positive relative to the TiO_2 layer.

The structural parameters reported for the samples in table 1 were assessed using DETAK profilometry measurements and SEM cross-section images. Blank samples (which were sprayed at the same time as the actual working samples) were used to determine the thickness of the dense TiO_2 and In_2S_3 buffer layers. All 11 samples were characterized with current–voltage (IV) measurements both in the dark and under illumination. IV measurements were acquired using a Princeton Applied Research 273 potentiostat/galvanostat. AM 1.5 measurements were acquired using a calibrated solar simulator (Solar Constant 1200, K.H.

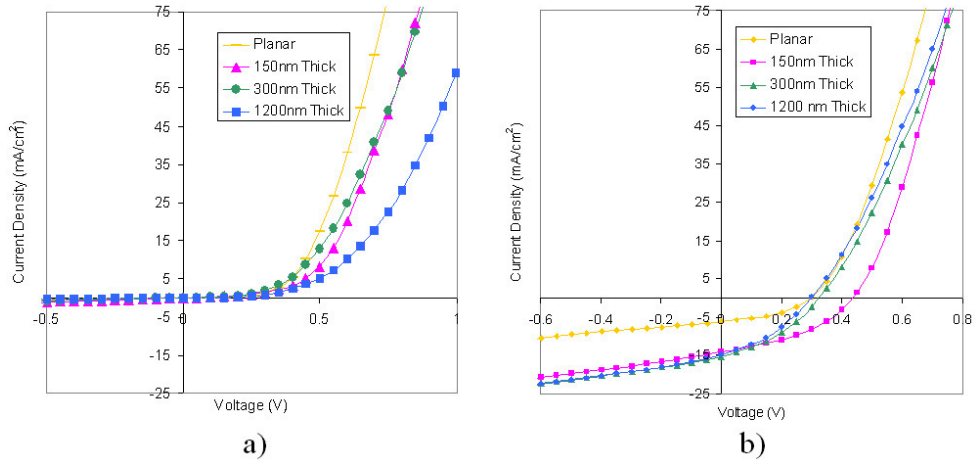

Figure 2. *IV* curves in the dark (a) and under AM 1.5 simulated irradiation (b) for the planar, 150 nm thick, 200 nm thick, and 1200 nm thick TiO_2/In_2S_3/CIS nanocomposite solar cell samples (samples 1–4 in table 1). Nanostructuring significantly improves the short circuit current density compared to the planar cell. Performance is maximized for the thinnest (150 nm) nanostructured layer. Solar cell performance characteristics extracted from these *IV* curves are summarized in table 2.

Table 1. Structural details of the 11 solar cell samples used for this parametric study.

Sample no	Sample ID	nc-TiO_2 thickness (nm)	nc-TiO_2 particle size (nm)	In_2S_3 buffer thickness (nm)	Dense TiO_2 layer thickness (nm)	$CuInS_2$ thickness (nm)
1	Planar	0	NA	50	150	1000
2	150 nm thick	150	300	50	150	1000
3	300 nm thick	300	300	50	150	1000
4	1200 nm thick	1200	300	50	150	1000
5	9 nm particles	200	9	50	150	1000
6	50 nm particles	200	50	50	150	1000
7	300 nm particles	200	300	50	150	1000
8	No buffer	200	300	0	150	1000
9	20 nm buffer	200	300	20	150	1000
10	60 nm buffer	200	300	60	150	1000
11	200 nm buffer	200	300	200	150	1000

Steuernagel Lichttechnik GmbH). IPCE measurements were acquired by measuring the wavelength dependence of the incident photon-to-current conversion efficiency using light from a 400 W halogen lamp (Oriel Inc.) focused onto the cell through a wavelength tunable monochromator (Acton Research Corp. Spectra-Pro 275). The monochromator was incremented through the visible spectrum to generate the IPCE(λ) curve. Because of the small electrode area used in these studies, *IV* and IPCE measurements were performed both with and without a mask to determine if a significant spreading current contributed to the measured results. In all cases, the measurements with and without a mask differed by less than 5%. For consistency, all results presented in this paper are for the mask-free measurements.

3. Results and analysis

The results of the nanoporous TiO_2 layer thickness study, TiO_2 nanoparticle size study, and In_2S_3 buffer layer thickness study are summarized in figures 2–4, respectively. Each of these three parametric studies will be discussed in detail below. To facilitate this discussion, the *IV* characteristics presented in figures 2–4 have been analysed in further detail using a modified diode-equation approach that allows both series resistance (R) and shunt (G) conductance losses to be quantified [19]:

$$J = J_o \exp\left[\frac{q}{AkT}(V - RJ)\right] + GV - J_L. \qquad (1)$$

In this equation, A is the diode ideality factor, q is the electron charge, k is Boltzmann's constant, T is temperature, J_L is the light current, and J_o is the reverse saturation current. Applying equation (1) to the *IV* data presented in figures 2–4 permits values for R, G, A and J_o to be extracted for all 11 samples both in the dark and under illumination. A graphical example of this analysis is shown in figure 5 for sample no 2. The end results of this analysis for all 11 samples are summarized in table 2. The best overall device (sample no 10) achieved 3.0% efficiency at AM 1.5. As documented in table 1, this sample had a TiO_2 matrix thickness $\approx$200 nm, TiO_2 nanoparticulate size = 300 nm, and In_2S_3 buffer layer thickness $\approx$60 nm.

3.1. Effect of TiO_2 nanoparticulate layer thickness

Figure 2 shows the effect of TiO_2 nanoparticulate layer thickness on *IV* performance in the dark (a) and under illumination (b) for an otherwise identical set of solar cell devices (samples 1–4 in table 1.) To ensure comparability, all four samples were fabricated at the same time in a single

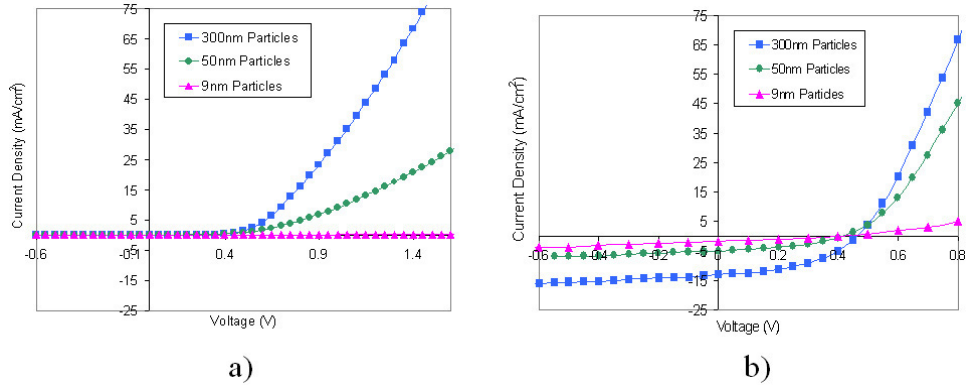

Figure 3. *I V* curves in the dark (a) and under AM 1.5 simulated irradiation (b) for the 9, 50, and 300 nm particle size TiO_2/In_2S_3/CIS nanocomposite solar cell samples (samples 5–7 in table 1). Performance increases with increasing TiO_2 nanoparticle size. Solar cell performance characteristics extracted from these *I V* curves are summarized in table 2.

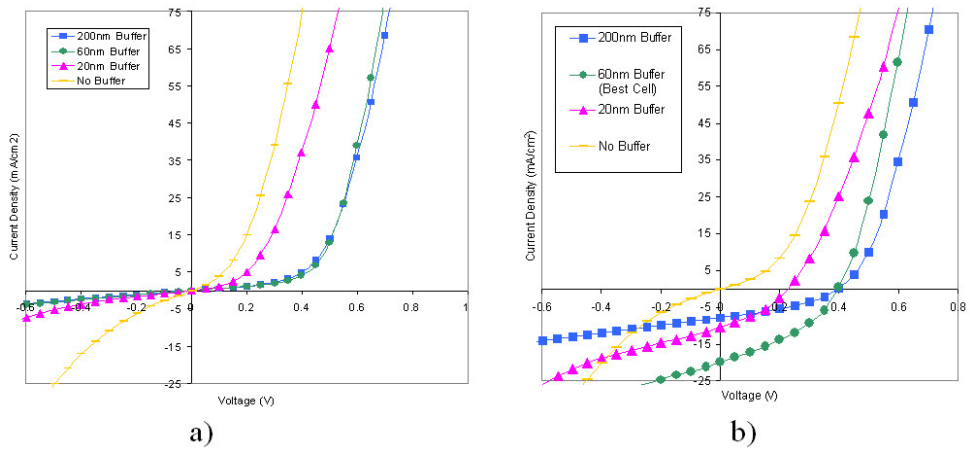

Figure 4. *I V* curves in the dark (a) and under AM 1.5 simulated irradiation (b) for the 0, 20, 60, and 200 nm thick buffer layer TiO_2/In_2S_3/CIS nanocomposite solar cell samples (samples 8–11 in table 1). Use of the buffer layer significantly improves performance. Performance is maximized for the intermediate thickness (60 nm) buffer layer. Solar cell performance characteristics extracted from these *I V* curves are summarized in table 2.

Table 2. *I V* analysis summary of the 11 solar cell samples used for the parametric study.

Sample no	Sample ID	J_{sc} (mA cm^{-2})	Voc (V)	FF	η (%)	G_{dark} (mS cm^{-2})	G_{light} (mS cm^{-2})	$R_{s,dark}$ (Ω cm^2)	$R_{s,light}$ (Ω cm^2)	A_{dark}	A_{light}
1	Planar	6.24	0.31	0.41	0.80	0.9	7.2	2.5	2.8	2.1	2.0
2	150 nm thick	14.0	0.45	0.40	2.5	2.2	14	3.1	2.4	2.1	2.0
3	300 nm thick	13.7	0.30	0.44	1.8	1.2	18	3.4	3.0	3.2	3.7
4	1200 nm Thick	8.60	0.32	0.34	0.9	0.9	20	3.9	3.0	4.1	3.6
5	9 nm particles	1.7	0.41	0.30	0.2	0.02	3.3	680	83	4.3	3.5
6	50 nm particles	5.0	0.41	0.40	0.8	0.2	4.0	5.5	3.4	3.6	3.8
7	300 nm particles	13.2	0.46	0.46	2.8	0.3	5.1	5.5	2.6	2.9	3.7
8	No buffer	0.05	0.02	0.25	0.0	22	28	1.4	1.3	2.6	2.9
9	20 nm buffer	9.70	0.22	0.38	0.8	8	26	1.7	1.6	2.6	2.9
10	60 nm buffer	19.8	0.40	0.38	3.0	6	24	1.5	1.6	1.85	1.8
11	200 nm buffer	7.80	0.40	0.36	1.1	5	11	2.0	1.7	1.85	1.8

batch. All samples (other than the planar sample) had the same 300 nm TiO_2 paste; only the thickness of this layer was varied. All other cell parameters (TiO_2 dense layer thickness, cell size, CIS layer thickness, buffer layer thickness) were held constant as indicated in table 1.

All three cells with the nanoporous TiO_2 layer showed markedly higher short circuit current densities compared to the planar cell, ($\sim$15 mA cm^{-2} compared to $\sim$5 mA cm^{-2}), indicating that nanostructuring substantially improved the incident photon to current conversion efficiency. The cell with a 150 nm nanoparticulate TiO_2 layer thickness exhibited the best overall performance. Further increasing the nanoparticulate TiO_2 layer thickness negatively impacted performance by decreasing the open circuit voltage and the fill factor.

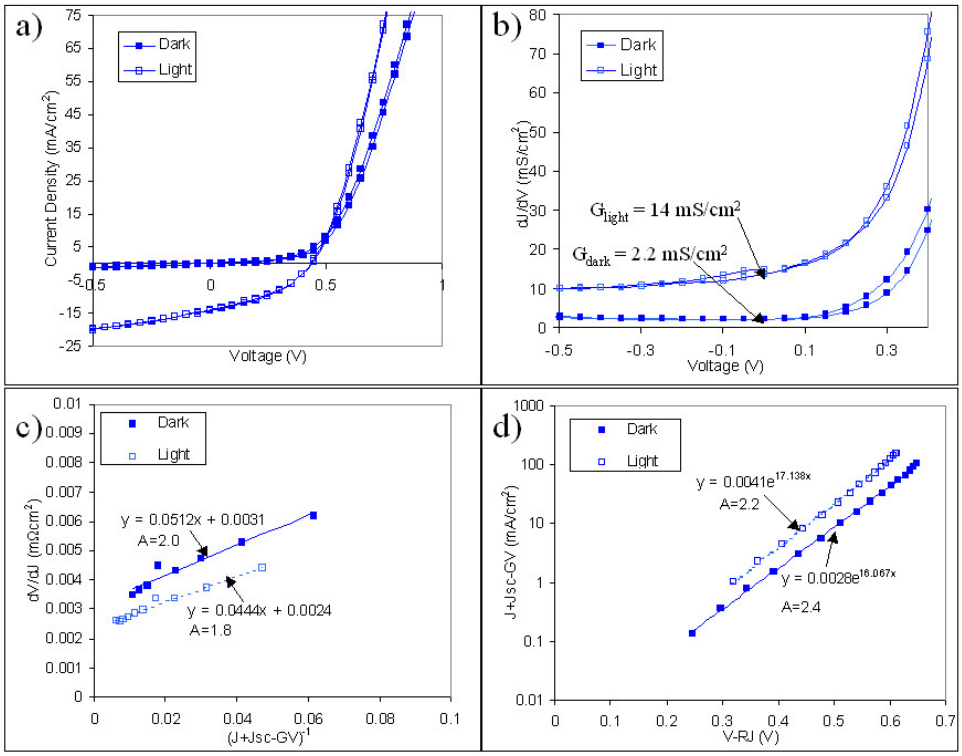

Figure 5. Example of the graphical analysis used to extract the IV parameters presented in table 2. The graphs in this figure are based on the dark and light IV data extracted from solar cell sample #2. (a) Original IV data in the dark (filled squares) and under AM 1.5 illumination (open squares) for solar cell sample #2. (b) A plot of $\mathrm{d}J/\mathrm{d}V$ versus voltage based on the IV data permits identification of G_{dark} and G_{light}. (c) A plot of $\mathrm{d}J/\mathrm{d}V$ versus the light and shunt corrected current density permits identification of R_{dark} and R_{light}. (d) A diode plot of the light and shunt corrected current density versus the IR corrected voltage allows the diode quality factor to be extracted from an exponential fit.

The quantitative IV analysis results summarized in table 2 (samples 1–4) provide further insight into the effect of TiO_2 nanoparticulate layer thickness. Most notably, the series resistance in the dark and under illumination (R_{dark} and R_{light}) and the shunt conductance under illumination (G_{light}) all increase with increasing nanoparticulate layer thickness. At the same time, the diode quality degrades with increasing nanoparticulate layer thickness. Increases in R_{dark} and R_{light} may be attributed to the increasing thickness of the nanoparticulate film (resulting in an increased average conduction path length for electrons), although the increase does not appear to scale linearly with layer thickness. The increase in G_{light} and the degradation in the diode quality factors likely reflect the increasing interfacial surface area associated with an increasing nanoparticulate film thickness. In combination, all of these factors contribute to a decrease in OCV and fill factor with increasing film thickness, eventually offsetting the initial enhancement in current collection provided by nanostructuring. The fact that the efficiency of the nanostructured cell manifests a maximum as a function of film thickness is not surprising considering the competing effects of light-induced charge carrier collection and recombination. In fact, an analytical assessment of a nanorod solar cell geometry has recently been published by Kayes *et al* [20], which discusses this effect in detail. They note that the efficiency of a planar solar cell will reach a limiting value as the thickness increases, but a nanorod cell will attain a maximum efficiency as a function of thickness. This effect is simply understood by remarking that the light generated current density (J_{l}) goes as:

$$J_{\mathrm{l}} \propto (1 - \mathrm{e}^{-\alpha L}), \tag{2}$$

where α is the absorption coefficient of the material, and L is the cell thickness, while the dark current (J_o) goes as:

$$J_o \propto L. \tag{3}$$

Thus, the competition between these two effects sets the optimum thickness for a nanostructured cell.

3.2. *Effect of TiO_2 nanoparticle size*

Figure 3 shows the effect of TiO_2 nanoparticle size on IV performance in the dark (a) and under illumination (b) for an otherwise identical set of solar cell devices (samples 5–7 in table 1.) To ensure comparability, all three samples were fabricated at the same time in a single batch. All samples had the same thickness nanoporous TiO_2 layer; only the size of the nanoparticles used in this layer was varied. All other cell parameters (TiO_2 dense layer thickness, cell size, CIS layer thickness, buffer layer thickness) were held constant as indicated in table 1.

In this parametric study, short circuit current increases markedly with increasing TiO_2 nanoparticle size. This change is accompanied by a commensurate increase in fill factor, and a slight improvement in OCV. All three factors contribute

to a significant improvement in efficiency with increasing TiO_2 nanoparticle size. Among the three samples, the cell with 300 nm TiO_2 nanoparticles exhibited the best overall performance.

The quantitative IV analysis summarized in table 2 (samples 5–7) provides further insights into the effect of TiO_2 nanoparticle size. Most notably, the series resistance in the dark and under illumination (R_{dark} and R_{light}), decrease significantly with increasing TiO_2 nanoparticle size. Charge transport in nanoparticulate TiO_2 is believed to be limited primarily by an interparticle hopping process [13]. Although the thickness of the nanoparticulate film is identical for all three samples in this study, the film composed of 9 nm TiO_2 particles will possess a greatly increased number of interparticle impediments. The increase in particle–particle junctions in the 9 nm sample compared to the 50 nm sample compared to the 300 nm sample is reflected by the commensurate increase in the magnitude of the R_{dark} element.

In addition to introducing more interparticle barriers, it might be expected that reducing the TiO_2 particle size could also alter defect density concentrations, average doping levels, or even the mechanism of charge transport. In spite of this expectation, initial studies on model air-filled TiO_2 nanostructures indicate that the average donor density levels and charge-transport mechanisms are almost identical between the small (9 nm) and large (300 nm) TiO_2 nanoparticle matrices [14]. Thus, although resistance increases in the 9 nm-based films, the overall mechanics of charge transport appear to remain the same.

Somewhat surprisingly, G_{dark} and G_{light} are observed to decrease with decreasing particle size, although one would initially expect that the higher surface area presented by smaller particle sizes should lead to an increase in G. A possible explanation is provided by SEM cross-section analysis of the solar cell devices (not shown), which reveals that the CIS layer infiltrates far more effectively into the 300 nm solar cell sample compared to the 9 nm solar cell sample. The larger particle size film therefore actually possesses a larger interfacial junction area, likely leading to the increased shunt conductance. These effects and further details about the particle-size dependent hopping-transport process are explored in more detail in [13] and [14].

If performance steadily improves as the particle size is increased from 9 to 300 nm, then would even larger particle sizes further improve performance? The three particle sizes examined in this study were constrained by the selection of commercially available precursor pastes. However, if larger anatase-TiO_2 particle sizes were available, what would be a reasonable upper bound particle size? We can arrive at a reasonable upper limit for the maximum practical TiO_2 particle size by considering the optical absorption length of CIS. The optical absorption coefficient of CIS is approximately 2×10^5 cm^{-1}, indicating that approximately 90% of incident light is absorbed by a 1 μm thick layer of CIS. Since the CIS layer need not be greater than 1 μm thick to collect most of the incident light, the underlying TiO_2 nanoparticles should also not exceed this size scale. Furthermore, when the TiO_2 particle size is on the same scale as the length of visible light, beneficial light trapping and scattering effects may also occur, enhancing solar cell performance. For these reasons, it is reasonable to propose that TiO_2 particles sizes up to, but not greater than approximately 1 μm may be appropriate for 3D nanostructured CIS/TiO_2 solar cell devices.

3.3. Effect of In_2S_3 buffer layer thickness

Figure 4 shows the effect the In_2S_3 buffer layer thickness on IV performance in the dark (a) and under illumination (b) for an otherwise identical set of solar cell devices (samples 8–11 in table 1). To ensure comparability, all four samples were fabricated at the same time in a single batch. All samples had identical thickness nanoporous TiO_2 layers made from the same 300 nm TiO_2 precursor paste; only the thickness of the In_2S_3 buffer layer deposited on top of the nanoporous TiO_2 layer was varied. All other cell parameters (TiO_2 dense layer thickness, cell size, CIS layer thickness) were held constant as indicated in table 1.

Short circuit current density first increases, attains a maximum, and then decreases, as buffer layer thickness is increased from 0 to 200 nm. Over the same range, OCV, fill factor, and diode quality increase with increasing buffer layer thickness before levelling off. These factors combine to produce a maximum in performance for the 60 nm buffer thickness sample, due predominantly to the maximal short circuit current density achieved at this thickness. The 60 nm buffer thickness sample yields the highest overall performance of the 11 samples tested in this paper, with an AM 1.5 efficiency of approximately 3%.

An examination of the quantitative IV results summarized in table 2 (samples 8–11) shows that both G_{dark} and G_{light} decrease with increasing buffer layer thickness, indicating that the buffer layer provides shunt passivation. At the same time however, R_{dark} and R_{light} trend slightly upwards, reflecting increased series resistance due to the buffer film. While the increasing series resistance will decrease performance, this effect alone does not explain why the short circuit current plummets as the buffer layer thickness is increased beyond 60 nm. However, the incident photon to current conversion (IPCE) comparison given in figure 6 provides further clues. In this figure, the IPCE response for the 60 nm thick buffer layer sample is compared to the IPCE response for the 200 nm thick buffer layer sample. The IPCE spectrum for the 200 nm buffer layer sample shows an abrupt drop-off below approximately 550 nm wavelength. The wavelength of this cut-off corresponds closely to the band-gap of In_2S_3 ($E_g \sim$ 2.2 eV) [21, 22]. Since In_2S_3, like CIS, has a large optical absorption coefficient, the 200 nm buffer layer is sufficiently thick to absorb a significant fraction of the incident light at wavelengths below 550 nm. These photons are prevented from reaching the CIS layer and are dissipated by recombination processes in the In_2S_3 rather than contributing to photocurrent. The optimal buffer layer thickness must therefore represent a compromise between sufficient interface passivation (as measured by the shunt conductance and diode quality factor) and sufficient optical transparency. Improving the quality of the buffer layer (by minimizing thickness inhomogeneities and pinholes) and/or increasing the buffer layer band-gap may lead to improved performance.

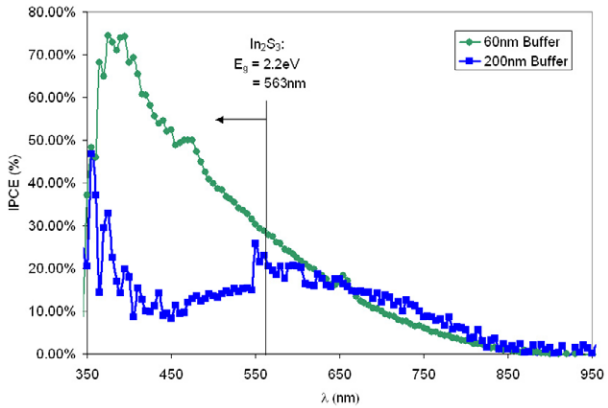

Figure 6. Incident photon to current efficiency (IPCE) spectra from the 60 nm thick buffer and 200 nm thick buffer solar cell samples. At wavelengths below approximately 550 nm, the IPCE signal from the 200 nm thick buffer sample suffers an abrupt reduction, corresponding closely to the band-gap of In_2S_3.

4. Conclusions

This parametric study clearly indicates that the performance of nanostructured $TiO_2/In_2S_3/CuInS_2$ solar cells depends strongly on geometric factors. TiO_2 particle size, TiO_2 matrix thickness, and In_2S_3 buffer layer thickness all play a critical role in determining solar cell performance. Optimization requires a delicate balance between the beneficial and deleterious effects caused by the TiO_2 nanostructuring. On the one hand, nanostructuring is beneficial because it increases charge carrier separation and decreases the probability of bulk recombination. This is because nanostructuring the p–n interface ensures that most charge carriers are created within a single diffusion distance of the interface, meaning that they can be split before recombining in the bulk. However, the disorder created by the nanostructuring is problematic because it decreases the efficiency of charge transport and increases the probability of interfacial recombination. This is because disordered nanostructuring introduces barriers to charge transport (such as dead-ends or particle-necks) and dramatically increases the amount of interfacial surface area available for interfacial recombination. Thus, randomized nanostructuring is a double-edged sword.

In the future, *ordered* nanostructuring may provide an intriguing alternative. This can potentially be accomplished by transitioning from a TiO_2 nanoparticulate design to a TiO_2 nanowire array design. Ideally, an ordered nanowire design would comprise an ordered array of thin n-type TiO_2 nanowire collectors spaced exactly two diffusion lengths apart. Compared to the disordered nanoparticulate design, the ordered nanowire array design would ensure efficient separation and collection of all charge carriers while dramatically improving charge transport and simultaneously minimizing the surface area for recombination.

In fact, working nanowire solar devices have recently been demonstrated in the dye-sensitized solar cell (DSSC) configuration [23–26]. These demonstrations prove the feasibility of the nanowire geometry. However, DSSCs fail to benefit from the reduced surface area presented by a nanowire geometry. This is because DSSCs need an extremely high surface area in order to support sufficient dye-density to absorb most of the incoming sunlight. The reduced surface area presented by a nanowire geometry is therefore a *disadvantage* for DSSCs; in a nanowire configuration, DSSCs no longer have sufficient dye area to absorb enough sunlight. In contrast to DSSCs, $TiO_2/CuInS_2$ nanocomposite solar cells would *strongly benefit* from the reduced surface area presented by a nanowire array. This is a topic of ongoing current research.

Acknowledgment

This material is based upon research supported by the National Science Foundation under Grant No. 0401817.

References

[1] O'Regan B and Grätzel M 1991 *Nature* **353** 737–40
[2] Pei Q, Yu G, Zhang C, Yang Y and Heeger A J 1995 *Science* **270** 719
[3] McFarland E W and Tang J 1999 *Nature* **421** 616–8
[4] Bach U, Lupo D, Comte P, Moser J E, Weissörtel F, Salbeck J, Spreitzer H and Grätzel M 1998 *Nature* **395** 583–5
[5] Wang P, Zakeeruddin S M, Moser J E, Nazeeruddin M K, Sekiguchi T and Grätzel M 2003 *Nat. Mater.* **2** 402–7
[6] Taretto K and Rau U 2004 *Prog. Photovolt.* **12** 573
[7] Ernst K, Belaidi A and Konenkamp R 2003 *Semicond. Sci. Technol.* **18** 475
[8] Rost C, Ernst K, Siebentritt S, Könenkamp R and Lux-Steiner M C 1998 *Proc. 2nd World Conf. Photovol. Sol. Ener. Conv. (Vienna)*
[9] Möller J, Fischer Ch-H, Siebentritt S, Könenkamp R and Lux-Steiner M Ch 1998 *Proc. 2nd World Conf. Photovol. Sol. Ener. Conv. (Vienna)*
[10] Nanu M, Schoonman J and Goossens A 2003 *Adv. Mater.* **16** 453
[11] Lenzmann F, Nanu M, Kijatkina O and Belaidi A 2004 *Thin Solid Films* **451** 639
[12] Nanu M, Schoonman J and Goossens A 2005 *Nano Lett.* **5** 1716–9
[13] O'Hayre R, Nanu M, Schoonman J, Goossens A, Wang Q and Gratzel M 2006 *Adv. Funct. Mater.* **16** 1566
[14] O'Hayre R, Nanu M, Schoonman J and Goossens A 2007 *Chem. Mater.* submitted
[15] Asenjo B, Chaparro A M, Gutierrez M T, Herrero J and Klaer J 2005 *Sol. Energy Mater. Sol. Cells* **87** 647
[16] Saad M and Kassis A 2003 *Sol. Energy Mater. Sol. Cells* **79** 507
[17] Grasso C and Burgelman M 2004 *Thin Solid Films* **451/452** 156
[18] Oja I, Nanu M, Katerski A, Krunks M, Mere A, Raudja J and Gossens A 2005 *Thin Solid Films* **480** 82
[19] Hegedus S S and Shafarman W N 2004 *Prog. Photovolt.* **12** 155–76
[20] Kayes B M, Atwater H A and Lewis N S 2005 *J. Appl. Phys.* **97** 114302
[21] Rodriguez C M, Silver A T, Ortiz A and Juarez A S 2005 *Thin Solid Films* **480** 133
[22] Bhira L, Essaidi H, Belgacem S, Couturier G, Salardenne J, Barreaux N and Bernede J C 2000 *Phys. Status Solidi* a **181** 427
[23] Adachi M, Murata Y, Okada I and Yoshikawa S 2003 *J. Electrochem. Soc.* **150** G488–93
[24] Law M, Greene L E, Johnson J C, Saykally R and Yang P 2005 *Nat. Mater.* **4** 455
[25] Baxter J B and Aydil E S 2005 *App. Phys. Lett.* **86** 53114
[26] Mor G K, Shankar K, Paulose M, Varghese O K and Grimes C A 2006 *Nano Lett.* **6** 215